International Journal of Applied Glass Science

RESEARCH ARTICLE OPEN ACCESS

Strengthening Potentials of Lithium-Doped Soda–Lime–Silicate Glasses Through Surface Crystallization of Quartz-ss

Fabian Stoelzel[1,2,3] | Thorsten Gerdes[2,3]

[1]Stoelzle Oberglas GmbH, Köflach, Austria | [2]Keylab Glass Technology, Faculty of Engineering Science, University of Bayreuth, Bayreuth, Germany | [3]Technology Application Center Spiegelau, Deggendorf Institute of Technology, Deggendorf, Germany

Correspondence: Fabian Stoelzel (Fabian.Stoelzel@uni-bayreuth.de)

Received: 25 July 2025 | **Revised:** 1 October 2025 | **Accepted:** 12 January 2026

Keywords: ion-exchange | quartz solid solution | soda-lime-silicate glass | strengthening | surface crystallization

ABSTRACT

The formation of a crystallized surface layer, having a lower coefficient of thermal expansion (CTE) than the parent glass, can be exploited to place the glass surface under compression during cooling from crystallization temperature and hence improve mechanical properties. In our study, we focused on the understanding of the compositional dependency of the surface crystallization of quartz solid solutions (Qz-ss) with potentially low CTE. Specifically, we investigated the crystallization of melt-prepared soda–lime–silicate glasses with variable Al_2O_3 content that were doped with lithium in exchange for sodium. Further, the role of ZnO and MgO in the crystallization was evaluated. Despite rather complex glass compositions, the observed cell parameters of the obtained Qz-ss are close to the corresponding ternary Li_2O—Al_2O_3—SiO_2 (LAS) system. Further, a simple model was applied to predict the in-plane stresses in the surface. For modeled compositions down to 5.5 mol% Al_2O_3, formation of a compressive layer for the complete range of the crystalline content can be observed. Our findings illustrate the potential of strengthening glasses through surface crystallization as an alternative to thermal- and chemical strengthening to make glass-packaging more weight competitive. The results can help to optimize glass compositions that can be strengthened by this method.

1 | Introduction

Glass is a popular packaging material with endless recyclability and outstanding properties, such as its chemical durability, which enables the packaging of food and pharma materials with a low risk of reactions of the goods with the container. However, with low resistance against breakage and high weight, glass packaging is less ideal than, for example, plastics or aluminum. Therefore, a reduction in wall thickness and weight through strengthening of the glass components would make glass more competitive. Despite the very high theoretical strength, the practical strength during usage is limited by flaws in the area of tensile stresses [1].

To obtain glass components with improved mechanical properties, glass surface modifications are used to suppress flaw formation and crack widening under load. Chemical strengthening is widely established for specialized applications, for example, display glass. For architectural glass, thermal strengthening is often applied. Both methods exploit the effect of the formation of a compressive outer layer, which counteracts the opening of cracks under load. Thus, an actual increase in the component's strength is possible. Achievable strength values range up to 400 MPa for thermal strengthening and up to 1000 MPa for chemical strengthening [2]. However, for container glass, both methods show some drawbacks. Thermal strengthening is carried out by rapid cooling

of the glass surface from above the glass transition temperature (T_g). This leads to a temperature gradient. The glass at the surface is transferred into an already "frozen state," while the interior can still relax stresses that have built up. Further cooling and complete "freezing" with a subsequent decrease in volume inside leads to the formation of compressive stress in the already rigid surface [3, 4]. To achieve the thermal gradient during cooling, a minimum homogeneous wall thickness and uniform cooling from all surfaces are required. Thermal strengthening is therefore technically difficult to implement for container glass and limited due to geometric aspects. Classical chemical strengthening is carried out by the exchange of ions (IOX) with larger radii for those with smaller ionic radius from the glass surface. Since the exchange is conducted well below T_g, the resulting compressive stress in the surface is only marginally reduced through relaxation [5]. Compared to thermal strengthening, a thinner and wall thickness independent surface layer with higher compressive stress is possible. Therefore, geometric limitations are almost completely eliminated. Ion-exchange typically is carried out by immersing parts in alkali nitrate melts at elevated temperatures for several hours [2, 6]. However, also other methods, such as the spraying of salts onto the glass surface and subsequent tempering, have also been described in the literature [7, 8]. Chemical strengthening is particularly effective for glasses from the aluminosilicate system. Soda–lime–silicate glasses, on the other hand, show lower performance due to faster stress relaxation during ion-exchange and lower diffusion rates [9–11]. With complex process control and relatively high treatment times, ion-exchange is realized mostly in a separate offline process.

Here, we exploit a third, less-studied approach, where the glass surface is set under compression by the formation of a partially crystallized surface layer with a coefficient of thermal expansion (CTE) lower than that of the parent glass [12–16]. This method regained interest in recent times through the combination of strengthening and higher wear resistance by an increase in surface hardness as a result of the presence of the crystalline phase [17, 18]. Flexural strengths of up to 800 MPa have been shown for glass compositions based on the lithium-aluminosilicate (LAS) system with high alumina contents through the surface crystallization of high-quartz solid solutions (HQz-ss) with extremely low CTE [16]. However, glass container production is negatively impacted by high alumina contents as a result of changes in meltability and viscosity [19, 20].

A more recent investigation of the ternary LAS system by Zandona et al. [21] determined the range of the CTE for the continuous quartz solid solutions (Qz-ss) series as a function of SiO_2/Al_2O_3 concentration (Al_2O_3 0–12.5 mol%). The gradual increase in the inversion temperature from high- to low-quartz solid solutions with a decreasing Al_2O_3 content (respectively increase of SiO_2) is responsible for the change of the overall CTE from room temperature (RT) to 573°C (i.e., the point of inversion for pure SiO_2 quartz). The study also shows that compositions with an Al_2O_3 content lower than the threshold to stabilize the HQz-ss can form crystalline phases with a mean overall CTE lower than for standard soda–lime–silicate glass (SLS).

In our study, the focus was to investigate how close compositions can be adapted to soda–lime–silicate container glass and yet being strengthened by the surface crystallization of Qz-ss.

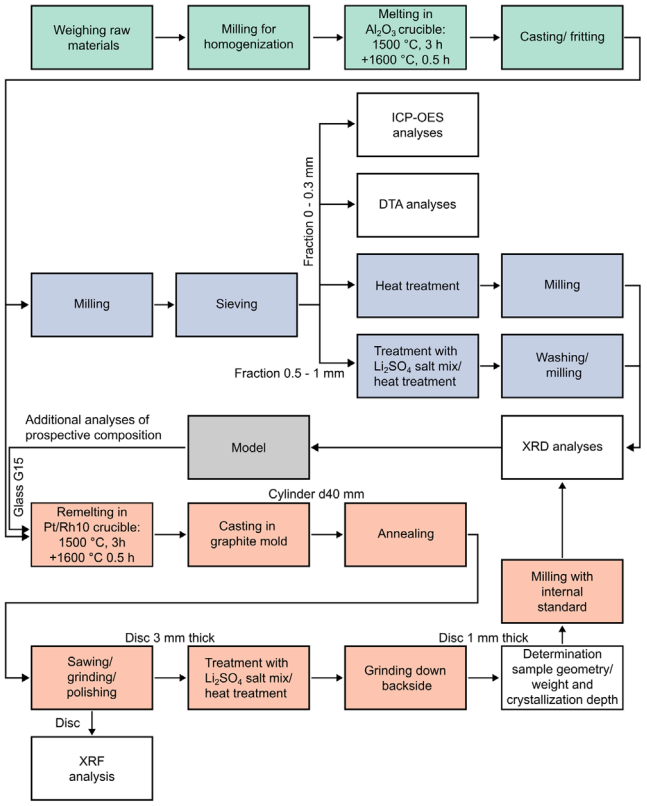

FIGURE 1 | Flow chart of the sample and material preparation.

First, we determined the influence of Li_2O, Na_2O, MgO, and ZnO on the crystallization using glasses produced by melt-quenching route. With the high cost of lithium in mind, we then focused on compositions with reduced lithium content. The influence of the SiO_2 and Al_2O_3 content on crystallization was therefore evaluated on glasses with low/no lithium content. For this purpose, they were subjected to ion-exchange with a lithium-containing salt mixture (based on Li_2SO_4) during the crystallization-inducing temperature program. Both crystallographic assessment by X-ray diffraction (XRD) of the crystallized glasses, and a model were used to predict the strengthening effects of the surface crystallization. In addition to the thermal expansion of the crystalline phase, we also particularly addressed the less-discussed aspect of the effect of the shift in the chemical composition in the residual glass during crystallization. Our approach can contribute to the development of glass components with improved mechanical properties, while maintaining meltability, processability, and costs at an acceptable level, making glass packaging more competitive compared to other materials.

2 | Methods

Figure 1 depicts an overview of the schematic material and sample presentation. Two different routes, the preparation of powders and the preparation of bulk samples, were chosen. Glasses were obtained by the classical melt-quench technique.

The examination was divided into different series of investigated glasses. *Series 1* was used to investigate the general influence

of additions of MgO and ZnO, respectively, their ratio on the crystallization of the system. Based on the findings, *Series 2* was designed to test the role of the Li_2O to Na_2O ratio and to evaluate a minimum viable Li_2O content to obtain a Qz-ss crystallization by the chosen thermal treatment. With *Series 3*, the influence of the Al_2O_3 to SiO_2 ratio on the variation of the cell parameters of the crystalline phase was investigated, and thermal expansion properties were derived. Given the found restrictions in Li_2O-content from *Series 2*, *Series 3*, with a lower internal lithium content, was subjected to ion-exchange with a lithium sulfate salt mix. From the results of *Series 3*, the potential strengthening effect was estimated by a model depending on the Al_2O_3 content of the glass and the fraction of the crystalline phase in the crystallized layer. Based on the findings, the most promising composition was identified, and the actual crystallization depth and crystallized volume fraction in the formed layer were determined.

2.1 | Batch Preparation and Glass Melting

Batches for glass melting were prepared from low iron quartz sand (Provodínské písky a.s, PR13), Al_2O_3 (Nabaltec, 99.8%), $CaCO_3$ (Thermo Scientific, 99.5%), $(MgCO_3)_4{\cdot}Mg(OH)_2{\cdot}5H_2O$ (Carl Roth, Ph. Eur., light), ZnO (Thermo Scientific, 99.9%), Li_2CO_3 (Carl Roth, 99%), Na_2CO_3 (Qemetica, granulated synthetic soda, calcined, 99.5%), and $KHCO_3$ (VWR Chemicals, 99.5%). The main constituents (by weight) of the quartz sand were determined to be 99.25% SiO_2, 0.28% Al_2O_3, and 0.13% K_2O. The batches were homogenized in a ZrO_2 planetary ball mill (PM100, Co. Retsch) for several minutes at 350 rpm. Batches then were melted in Al_2O_3 crucibles (Co. Porzellanfabrik Hermsdorf, 99.7%) in an electrical furnace (Carbolite BLF 17/8) under air.

The melting program was chosen to obtain glasses with a minimal amount of bubbles and sufficiently low viscosity during casting. First, the batch was heated to 900°C with a subsequent dwell time of 30 min for calcination and degassing of carbonates. Then the material was further heated to 1500°C and held for 3 h. Finally, heating to 1600°C with an additional dwell time of 30 min was carried out directly before casting. The glass melts were cast and fritted in DI water. On glass frit of composition G15 an additional melting in a Pt/Rh10 crucible was performed, using the same melting temperatures and dwell times, except that the calcination step at 900°C was omitted. A cylinder was produced by casting the molten glass into a preheated graphite mold with a diameter of 40 mm. The cast cylinder was transferred into an annealing oven and cooled at 570°C for 90 min.

The nominal compositions of the molten glasses by the batch compositions in mol% are displayed in Table 1.

2.2 | Sample Preparation

The prepared glass frits were milled in a ZrO_2 planetary ball mill, and different fractions were obtained by sieving. Samples for the investigation of the general crystallization tendency by XRD and Differential Thermal Analyses (DTA) without further lithium ion-exchange were obtained from powders of the fraction 0–300 µm. Four grams of each material were ceramized in small Al_2O_3 crucibles in a laboratory furnace (Nabertherm LH 216/12) with various programs, displayed in Table 2 (T1–T5, Glasses G01–G09). As partial sintering was observed, an additional milling step at low speed to avoid over-milling was conducted after the treatment to obtain powder samples for XRD evaluation. The thermal treatment for XRD samples was, in general, oriented on temperatures obtained from DTA measurement of glass powders G01–G05, lying between T_g and crystallization onset. Assuming a generally lower crystallization tendency for glasses G06–G09 by the lower Li-content, and thus also higher viscosity, a gradually increased treatment temperature with decreasing Li-content was chosen (T2–T5).

For the treatments by additional ion-exchange the particle fraction of 0.5–1 mm of glasses G10–G15 was used to enable later wash-off of the residual salt. 4 g of glass powder were mixed with 1 g of, in a pestle and mortar ground, dry salt mix ($87.5Li_2SO_4$—$11.5Na_2SO_4$—$1MgSO_4$ [mol%]) from $Li_2SO_4{\bullet}1H_2O$ (Carl Roth, >99% p.a.), Na_2SO_4 (Lenzing sodium sulfate SL, 99.8%), $MgSO_4{\bullet}7H_2O$ (Carl Roth, > 99% p.a.), placed in small Al_2O_3 crucibles and compacted. Additional 0.5 g of salt mix was used to cover the sample. The temperature program was conducted according to T6. Subsequently, material was cooled with natural cooling of the furnace. The salt after treatment was removed by adding 80 mL deionized (DI) water to the samples leaching them for 12 h and then rinsing several times with DI water. Then samples were dried at 105°C and milled to prepare powders for XRD investigation.

From the cast cylinder of glass G15, discs were cut with a diamond saw, ground to a thickness of 3 mm, and one side progressively polished down to 1 µm diamond suspension (Struers DP-Suspension P). On the polished side, a 1-mm thick layer of the dry salt mix ($87.5Li_2SO_4$—$11.5Na_2SO_4$—$1MgSO_4$ [mol%]) was applied by manually pressing to the surface. The sample was then subjected to thermal treatment T6 laying on a pressed alumina powder bed. The salt mix was designed so that the ion-exchange takes place at temperatures high enough to relax the initially formed tensile stresses due to the volume decrease by the smaller lithium ions. After cooling from treatment with natural cooling in the oven, the salt crust was washed off, and the untreated backside of the sample was further ground to obtain a final disc thickness of approx. 1 mm.

2.3 | Analytical Methods

The crystallization tendency of powders from glasses G01–G05 (fraction 0–300 µm) was investigated in differential thermal analysis (DTA) measurements (Netzsch STA 409) by heating 110 mg in alumina crucibles to 1300°C at 10 K/min in synthetic air versus an alumina reference.

Powders from thermally treated materials were investigated in X-ray diffraction measurements (XRD, Bruker D8 Discover A25, 1D Lynxeye detector, using Cu x-ray tube) in Bragg–Brentano configuration and pattern evaluated with Profex software [22]. All XRD measurements were performed at room temperature. Powders of glasses G01–G05 subjected to temperature program T1, and G10–G15 treated by Li-exchange and temperature program T6, were analyzed by using Le Bail refinement to obtain lattice parameters

TABLE 1 | Nominal compositions of molten glasses (mol%).

Series 1: Variations of MgO:ZnO ratios								
Glass composition G#	**SiO_2**	**Al_2O_3**	**CaO**	**MgO**	**ZnO**	**Li_2O**	**Na_2O**	**K_2O**
G01	66.2	7.4	7.1	2.1	4.0	9.0	4.0	0.2
G02	66.2	7.4	7.1	3.1	3.0	9.0	4.0	0.2
G03	66.2	7.4	7.1	4.1	2.0	9.0	4.0	0.2
G04	66.2	7.4	7.1	5.1	1.0	9.0	4.0	0.2
G05	66.2	7.4	7.1	6.1	0.0	9.0	4.0	0.2
Series 2: Variations of Li_2O:Na_2O ratios								
Glass composition G#	**SiO_2**	**Al_2O_3**	**CaO**	**MgO**	**ZnO**	**Li_2O**	**Na_2O**	**K_2O**
G02	66.2	7.4	7.1	3.1	3.0	9.0	4.0	0.2
G06	66.2	7.4	7.1	3.1	3.0	7.0	6.0	0.2
G07	66.2	7.4	7.1	3.1	3.0	5.0	8.0	0.2
G08	66.2	7.4	7.1	3.1	3.0	3.0	10.0	0.2
G09	66.2	7.4	7.1	3.1	3.0	1.0	12.0	0.2
Series 3: Variations of SiO_2:Al_2O_3 ratios								
Glass composition G#	**SiO_2**	**Al_2O_3**	**CaO**	**MgO**	**ZnO**	**Li_2O**	**Na_2O**	**K_2O**
G10	61.5	8.0	12.0	3.5	0.0	2.0	12.8	0.2
G11	62.5	7.0	12.0	3.5	0.0	2.0	12.8	0.2
G12	63.5	6.0	12.0	3.5	0.0	2.0	12.8	0.2
G13	64.5	5.0	12.0	3.5	0.0	2.0	12.8	0.2
G14	66.5	3.0	12.0	3.5	0.0	2.0	12.8	0.2
G15	66.6	6.0	10.0	3.5	0.0	0.0	13.8	0.0

TABLE 2 | Programs for thermal treatment of the glasses.

Thermal treatment	**Glass**	**Heating rate 1 (K/min)**	**Temperature 1 (°C)**	**Dwell time 1 (min)**	**Heating rate 2 (K/min)**	**Temperature 2 (°C)**	**Dwell time 2 (min)**
T1	G01 - G05	5	600	180	5	650	360
T2	G06	5	610	180	5	660	360
T3	G07	5	625	180	5	675	360
T4	G08	5	635	180	5	685	360
T5	G09	5	650	180	5	700	360
T6	G10 - G15	10	635	30	1	685	180

of the Qz-ss crystalline phase. The compositional dependency was evaluated versus the Al_2O_3 content of the glass, normalized to the ternary LAS system. The reference to the Al_2O_3 content was chosen based on technical considerations in terms of glass composition design. Further quantitative phase analysis of the Qz-ss of the surface crystallization of a bulk disc sample of G15 using an internal standard were conducted. The crystallization depth versus the total thickness was evaluated using optical microscopy on the cross-section obtained by breaking the disc. Based on sample mass determined on a fine balance (4 decimal digits), 10 wt.% of Y_2O_3 (Thermo Scientific, Reacton 99.9%) was added and milled with the sample for XRD testing.

In addition, the actual chemical compositions of glasses G10–G14 for the precise evaluation with special respect to the SiO_2 and Al_2O_3 content in the glasses were tested by ICP-OES analyses on powders (contracted measurement at IGR Institut für Glas- und Rohstofftechnologie, Göttingen, Germany), and for lithium-free glass G15 in XRF analysis (PANalytical Zetium, SST-R-mAX) on a prepared untreated bulk disc.

2.4 | Calculation of In-Plane Stresses in the Crystallized Surface Layer

Based on the difference in CTE of the crystallized layer and parent glass, the temperature-dependent equi-biaxial in-plane stress in the layer can be estimated according to [23]:

$$\sigma = \frac{E \cdot \Delta\alpha \cdot \Delta T}{1 - \nu} \quad (1)$$

with:

- $\Delta\alpha = \alpha_G - \alpha_{GC}$
- α_G: linear thermal expansion of parent glass
- α_{GC}: linear thermal expansion of crystallized layer as a function of linear thermal expansion of the crystalline phase α_C, volume fraction of crystalline phase n, and linear thermal expansion of residual glass α_{RG}
- ΔT: Temperature difference by the cooling from treatment temperature
- E_{GC}: Young's modulus of crystallized layer as function of Young's modulus of the crystalline phase E_C, volume fraction of crystalline phase n, Young's modulus of residual glass E_{RG}
- ν: Poisson's ratio for the crystallized layer

An additional coefficient of the ratio of the internal cross-section (uncrystallized area) A_i to the area of total cross-section A_t [16] was not considered in the equation, as no actual geometry was evaluated, and by the very thin crystallized layer compared to the uncrystallized thickness $A_i/A_t \approx 1$ is expected. An overview of the basic set of parameters used in the calculation is given in Table 3.

The following modeling assumptions were made:

- Only Qz-ss occurs as the sole crystalline phase. Minor impurities of other crystalline phases formed during crystallization are neglected.
- Formed layers are discrete and have isotropic properties.
- The thermo-mechanical properties follow a linear mixing rule by the volume fraction of crystallinity in the partially-crystallized layer.
- Stresses at treatment temperature equal zero.
- The cooling regime for stress calculation starts in the vicinity of T_g of the parent glass (560°C).
- No stresses are released during cooling, assuming a fast enough cooling from the upper temperature to well below strain point.
- Depletion of elements in the glass involved in crystallization leads to a changed composition and CTE of the residual glass phase (α_{GR}).
- CTE values of the materials are average values of the complete cooling regime.
- CTE values for the glassy parts are derived by calculations based on model by Appen [24]. As this model is specified for a temperature range of 20°C–400°C, the extrapolated values will show an underestimation for the larger overall temperature window.
- Ion-exchange from the outside is the faster mechanism and takes place before the crystallization. Denoted exchanged fractions are meant before the crystallization
- During crystallization, no more ion-exchange from outside takes place.
- Crystallization occurs in the given stoichiometry of the normalized Li_2O—Al_2O_3—SiO_2 system defined by the available SiO_2 and Al_2O_3 contents in the glass. A sufficiently high local available amount of Li^+ by diffusion to compensate charge of the $[AlO_4]^-$ units is assumed.
- No shift of the stoichiometry of the crystalline phase during crystallization takes place.

TABLE 3 | Basic set of parameters used in the calculation of the thermal stresses.

	Value	Reference
α_G	Dependent on glass composition	Estimated based on the Appen model [24]
α_C	Dependent on Qz-ss stoichiometry	Estimated based on considerations of the crystal unit cell investigation compared to data from Zandona et al. [21]
α_{GR}	Dependent on glass composition	Estimated based on residual glass composition from the Appen model [24]
α_{GC}	$= n \bullet \alpha_C + (1\text{-}n) \bullet \alpha_{RG}$	
ΔT	535 K	(560°C–25°C)
E_C	97 GPa	Based on data from Zerodur (90.3 GPa) [25], corrected by assumed 25% residual glass
E_{RG}	70 GPa	Based on Shelby [26] for standard SLS glass
E_{GC}	$= n \bullet E_C + (1\text{-}n) \bullet E_{RG}$	
ν	0.24	Based on data for Zerodur [25]

The calculation of the stress in the layer starts with the calculation of the CTE of the base glass composition. In the second step, the ion-exchange of sodium from the glass with lithium from an external salt is considered to have a certain exchanged fraction (e.g., 88%, predicted by the applied salt mix composition ratio of Li^+/Na^+) at the exchange surface. From the obtained and by the ion-exchange defined fictive glass composition, the crystalline phase with its stoichiometry multiplied by a molar factor is subtracted. This leads to the molar composition of the residual glass from which the CTE can be calculated. By the total molar parts crystallized and resulting molar parts of the residual glass of the oxides, the crystalline phase and residual glass phase

are transferred into weight parts. As the actual density of the crystalline phase is unknown, the interpolated XRD density (e.g., 2.47 g/cm^3 for crystallized G15) is used. From the weight parts and the densities, the volume fraction of the crystalline phase and the volume fraction of the residual glass can be obtained. Densities for the conversion of weight to volume fractions of the glassy parts were obtained by the Fluegel model [27]. The complete set of parameters is then used for an iterative calculation of the resulting compressive stress in the crystallized layer depending on the crystallized volume according to Equation (1). The compressive stresses are displayed to be negative, while tensile stresses are positive. Calculations and details can be found in Supporting Information S1. It shall be noted that for the sake of practicality and compliance with the literature, CTE values are meant to be referred to a reference length at RT.

In general, the calculated stress values are expected to have a relatively large uncertainty by the assumptions made and potential deviations of the input parameters. For example, a standard deviation for the Young's modulus of the crystallized layer in the range of ± 5 GPa, and a standard deviation of the Poisson's ratio of ± 0.03 already would lead to an overall standard deviation of about ± 20% for the calculated stresses. Therefore, the obtained values should be understood as an indication of the potential and to highlight the influencing factors.

3 | Results and Discussion

The glass formation of the different series was tested by XRD. Figure 2 shows measurements on as-quenched compositions representing the range and different series of the obtained glasses.

For the investigated glasses, only in the case of glass G10, a feature at about 30° two-theta was noticed that might be discussed as a hint of crystallization. However, subsequent heat treatment, as shown in the results of *Series 3*, did not result in any significant difference in the XRD characteristics for this composition compared to the other glasses.

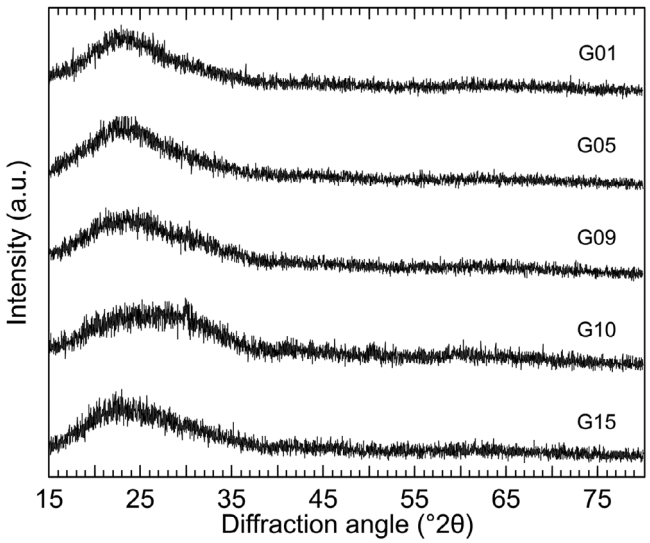

FIGURE 2 | XRD measurements on as-quenched glasses.

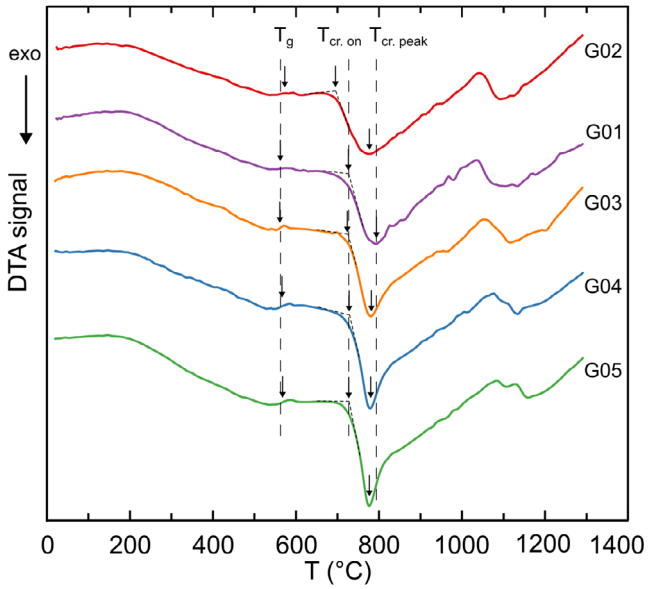

FIGURE 3 | DTA measurements of glass powders G01–G05 under heating at 10 K/min, exothermic reaction in downward direction. The glasses are sorted in ascending order by the prominence of the crystallization signal. Vertical dashed lines mark the position of the characteristic temperatures of glass G01 as a guide for the eye. The individual temperatures of each glass are marked by arrows.

TABLE 4 | Characteristic temperatures of glasses G01–G05 obtained in DTA measurements.

Glass	MgO:ZnO	Tg (°C)	T cryst. onset (°C)	T cryst. peak (°C)
G01	2.1:4.0	565	724	797
G02	3.1:3.0	577	695	776
G03	4.1:2.0	562	720	780
G04	5.1:1.0	570	725	778
G05	6.1:0	573	724	777

3.1 | Series 1: Variation of MgO:ZnO Ratios

Figure 3 shows the DTA analyses of glasses G01–G05, having a variation of the MgO to ZnO ratio. The obtained characteristic temperatures are presented in Table 4.

In the vicinity of the determined T_g values, further features can be found that might be attributed to another glass transition and thus potential phase separation.

The DTA analyses show the least prominent exothermic peak for the crystallization of glass G02 at a MgO to ZnO ratio of approx. 1:1. Increasing the ZnO content at the expense of MgO (Glass G01) or increasing the MgO at the expense of ZnO (Glasses G03–G05) away from the 1:1 ratio leads to a narrower and pronounced crystallization signal. With glass G05 containing only MgO species (i.e., no ZnO) showing the sharpest exothermic signal for the crystallization. All species Li^+, Mg^{2+}, and Zn^{2+} are

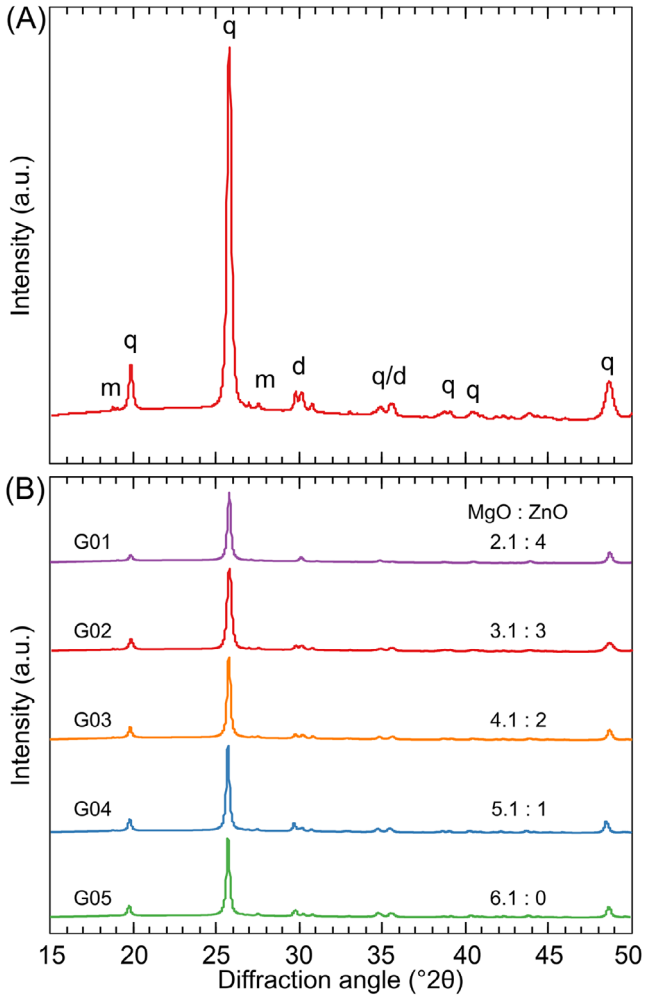

FIGURE 4 | XRD measurements of ceramized glass powders G01–G05. (A) Exemplary detail for glass G02 with attribution of the crystalline phases: *q* for Qz-ss, *d* for diopside, and *m* for lithium metasilicate. (B) Influence of the variation of MgO–ZnO content in the glasses.

known to be incorporated into Qz-ss, charge balanced by $[AlO_4]^-$ tetrahedral structural units [28–33].

The effect of the less prominent crystallization peak at the ratio Mg:Zn = 1, while having the lowest temperature for crystallization onset, is not fully understood but might be a result of concurring effects of diffusion and incorporation into the crystal structure comparable to mixed-alkali earth effects [34]. The evaluation of the heat-treated glass powders G01-G05 by XRD confirms the formation of Qz-ss as the predominant crystalline phase (based on COD pattern # 8104230) (Figure 4). Further detected minor phases are diopside and lithium metasilicate. Glasses with higher MgO content were found to have the tendency to provide a more pronounced diopside crystallization.

Le Bail refinements of the crystallized samples of G01–G05 show a tendency of a slight decrease in lattice parameter *c* and an increase in lattice parameter *a* with the increase of MgO content in the glass, replacing ZnO (Table 5).

This trend represents the intermediate behavior from the Qz-ss based on the pure LAS system with partial substitution

TABLE 5 | Lattice parameters and cell volumes for crystallized glass G01–G05.

Glass	Lattice parameter *a* (Å)	Lattice parameter *c* (Å)	cell volume *V* (Å ^{3})
G01	5.1482(9)	5.451(1)	125.12(7)
G02	5.152(1)	5.446(1)	125.2(1)
G03	5.155(1)	5.4471(8)	125.33(7)
G04	5.1597(8)	5.4443(7)	125.52(6)
G05	5.1626(8)	5.4459(8)	125.70(6)

Note: Numbers in parentheses provide the estimated standard deviation of the last digit.

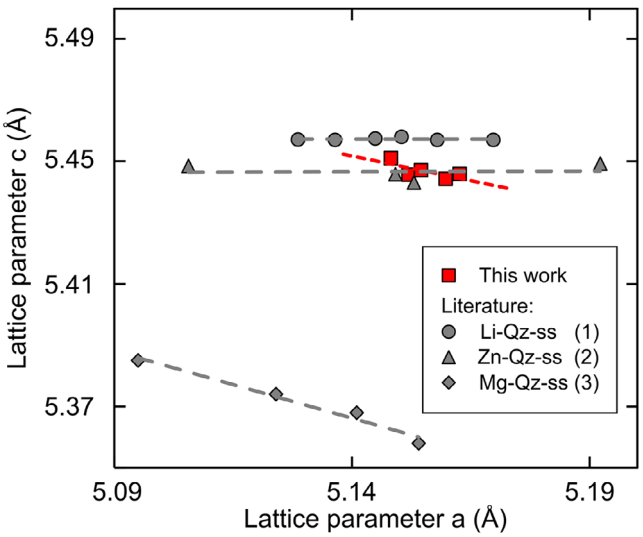

FIGURE 5 | Lattice parameters of the Qz-ss obtained for glasses G01–G05 heat-treated according T1 in comparison to Qz-ss phases obtained for pure LAS, ZAS, and MAS systems: Li-Qz-ss (1) [21], Zn-Qz-ss (2) [36], and Mg-Qz-ss (3) [35]. Linear fitting lines for guidance of the eye. Error bars are smaller than the depicted symbols.

of Li^+ by Zn^{2+} and (Li^+ + Zn^{2+}) by Mg^{2+} in the direction of the $MgO—Al_2O_3—SiO_2$ (MAS) system [21, 35, 36]. Figure 5 shows the dependency of cell parameter *c* on cell parameter *a* for the crystallized glasses G01–G05 in comparison to Qz-ss obtained from literature for the pure ternary LAS (Al_2O_3 content 9–12.5 mol%) [21], $ZnO—Al_2O_3—SiO_2$ (ZAS) (Al_2O_3 content 8.5–15 mol%) [36], and MAS system (Al_2O_3 content 12.5–19.5 mol%) [35].

Similarities in the behavior of the Li-Qz-ss and Zn-Qz-ss are result from the occupancy of Li^+ in the tetrahedral site of the crystal structure and the preference of Zn^{2+} for the tetrahedral site over the octahedral site [36], leading to a hexagonal crystal structure for the HQz-ss phase. Mg^{2+}, on the other hand, has been shown to establish a pseudo-hexagonal feature by the continuing tetrahedral tilt leading to a successive transition between low- and high quartz-like arrangements [30, 35]. However, compared to lithium, the effect of MgO and

ZnO on the crystallization in the investigated glasses is rather low.

3.2 | Series 2: Variation of Li_2O:Na_2O Ratios

The variation of Li_2O to Na_2O of glass G02 versus G06–G09 shows a higher crystallization tendency for higher Li_2O contents for the given individual heat treatment (T1–T5). It is found that the crystallization is limited to a Li_2O content of about 7 mol%. At 5 mol% for glass G07 for the specific thermal treatment (T3) no crystallization was obtained (Figure 6).

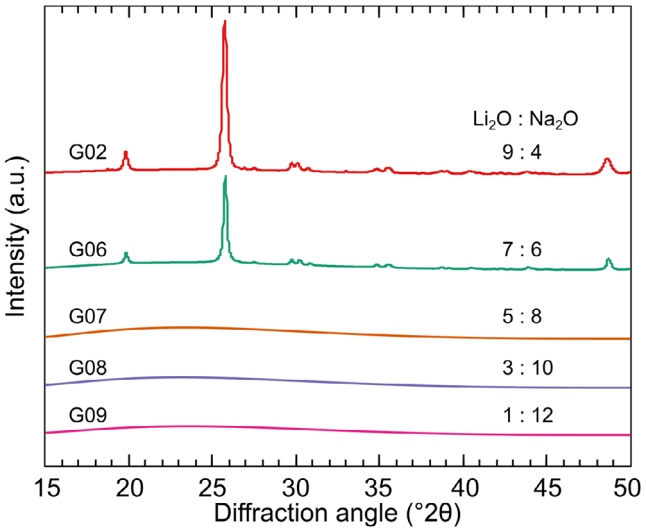

FIGURE 6 | XRD measurements of heat-treated glass powders G02, G06–G09 with variation of Li_2O to Na_2O ratios.

It is believed that this effect might be attributed to the lowered viscosity by lithium and therefore enabling crystallization at these relatively low treatment temperatures. In addition, it is expected that lower amounts of lithium in comparison to the favored stoichiometric range for the Qz-ss formation lower the total amount of potentially formed crystalline phase. Further, a slight excess of lithium has been reported to improve the crystallization tendency [37].

3.3 | Series 3: Variation of SiO_2:Al_2O_3 Ratios

In the discussed glass compositions G01–G09 of *Series 1 and 2*, the main cost driver for the formulation is the lithium component, followed by ZnO. As shown in the DTA and XRD measurements, ZnO and MgO lead to rather small deviations in the overall crystallization characteristic. For glasses G10–G15, therefore, the approach was chosen to eliminate ZnO from the composition and drastically decrease the Li_2O content.

To account for possible changes in alumina content due to the melting process, the exact chemical composition (G10–G15) was analyzed. Table 6 shows the actual compositions of glasses G10–G15 obtained by chemical analyses.

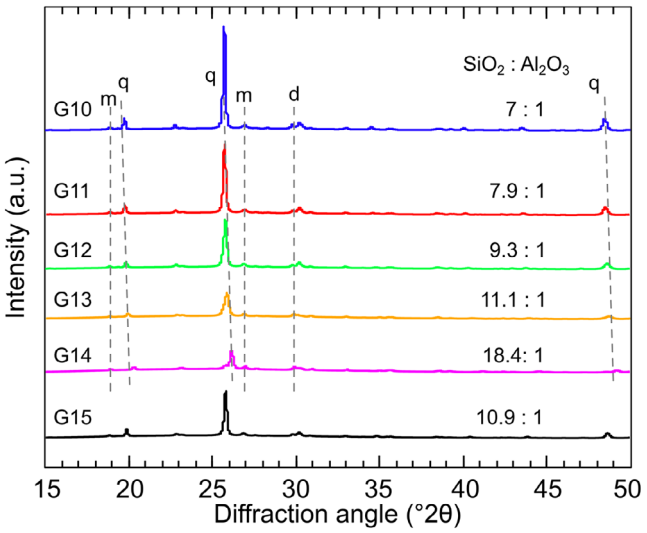

FIGURE 7 | XRD measurements for crystallized glass powders G10–G015 with variation of SiO_2 to Al_2O_3 ratios, *q* for Qz-ss, *d* for diopside, and *m* for lithium metasilicate.

Slight deviations from the nominal glass compositions were found to occur and are expected to originate from intrusion of Al_2O_3 from crucible material, residual moisture on raw materials, and evaporation of alkali. To maintain a sufficient availability of lithium for the crystallization, it was supplied by external ion-exchange on glass powders.

The following phases were detected in XRD measurements for glasses G10–G15 crystallized according to thermal treatment T6: Qz-ss as the main phase, minor amounts of Li-metasilicate, and diopside. Further impurities of metathenardite from residual Na_2SO_4 by the salt treatment were partially found. Even for an Al_2O_3 content as low as 3.6 mol%, the crystallization of the Qz-ss was evident for glass G14 and the given thermal treatment (Figure 7).

The lattice parameters obtained by Le Bail refinement for the Qz-ss crystal phases of the analyzed powders show an intermediate behavior between the lattice parameters known from the literature for the pure LAS and MAS systems [21, 35] (Table 7 and Figure 8).

Although the tendency is toward the LAS system, it is believed that other elements present in the glass, especially Mg^{2+}, are incorporated into the crystal structure to a lesser extent, leading to the deviations from the pure LAS system (Figure 9).

Assuming a hexagonal crystal structure for the HQz-ss and a trigonal crystal structure for LQz-ss [31], the unit cell volumes for the crystalline phases are derived. From the analyses of the glass compositions, a normalized molar ratio of SiO_2—Al_2O_3—Li_2O, accessible for the crystallization, was calculated. It is assumed that enough lithium (and further Mg^{2+}) is locally available, present from the ion-exchange, for the charge compensation of the stoichiometry $Al_2O_3/(Li_2O + MgO) = 1$.

The linearized average cell lengths $\sqrt{V}$ were normalized to one at an Al_2O_3 content of 11.1 mol% of the LAS system. Cell

TABLE 6 | Compositions of glasses G10–G15 by chemical analyses.

Glass composition G# (mol%)	SiO_2	Al_2O_3	CaO	MgO	ZnO	Li_2O	Na_2O	K_2O
G10	60.5	8.6	12.2	3.7	0.0	1.8	13.0	0.2
G11	61.3	7.8	12.3	3.7	0.0	1.8	12.9	0.2
G12	62.6	6.7	12.3	3.7	0.0	1.8	12.7	0.2
G13	63.5	5.7	12.4	3.7	0.0	1.8	12.7	0.2
G14	66.2	3.6	12.2	3.7	0.0	1.8	12.3	0.2
G15[a]	66.6	6.1	9.9	3.6	0.0	0.0	13.8	0.0

[a]by XRF analysis.

TABLE 7 | Lattice parameters and parameter-dependent values for crystallized glasses G10–G15 with SiO_2, Al_2O_3, and Li_2O contents normalized to the LAS system based on analyzed compositions.

	Normalized value (mol%)							
Glass	SiO_2	Al_2O_3	Li_2O (+MgO)	Lattice parameter *a* (Å)	Lattice parameter *c* (Å)	Cell volume *V* (Å^3)	Average cell length $\sqrt{V}$ (Å)	Normalized linearized length
G10	77.9	11.1	11.1	5.2039(3)	5.4368(3)	127.51(2)	5.0332(3)	1
G11	79.7	10.1	10.1	5.1895(4)	5.4387(5)	126.84(3)	5.0245(4)	0.9983
G12	82.4	8.8	8.8	5.1702(6)	5.4397(7)	125.93(5)	5.0123(6)	0.9959
G13	84.8	7.6	7.6	5.1447(1)	5.4408(1)	124.71(1)	4.9962(1)	0.9926
G14	90.2	4.9	4.9	5.061(1)	5.4356(1)	120.56(5)	4.9401(7)	0.9815
G15	84.6	7.7	7.7	5.1541(5)	5.4459(5)	125.28(4)	5.0038(5)	0.9942

Note: Numbers in parentheses provide the estimated standard deviation of the last digit.

volumes from literature were used to derive linearized average cell lengths of the pure LAS system normalized to one at an Al_2O_3 content of 11 mol% [21] (Figure 10A). Despite the found slight difference in lattice parameters for the investigated glasses, the overall composition-dependent change in the relative average cell lengths measured at RT shows a comparable behavior, especially for the HQz-ss regime, to the pure LAS system from literature. This indicates that, also for these multicomponent glasses, the stoichiometry of the formed Qz-ss is mainly a result of the SiO_2 to Al_2O_3 ratio in the glass, given that a sufficient amount of Li^+ is locally available for charge balance.

Also from literature, it is known that for the LAS system, an approximated SiO_2 content smaller than ~82.5 mol%, respectively Al_2O_3 and Li_2O content of at least 8.75 mol% each, are able to stabilize the HQz-ss phase down to RT. Lower Al_2O_3 values result in a shift of inversion temperature to higher temperatures [21, 38]. The pronounced decrease of the normalized mean cell lengths in the LQz-ss regime by the decreased Al_2O_3 content is a direct result of the collapse of the cell volume by the inversion from HQ to LQ with a gradual shift to higher temperatures. Another effect of the volume change is the change in density following the inverse behavior (Figure 10B). The shift of the inversion temperature to above room temperature is depicted by the change in the slope of the curve of the properties. The overall thermal expansion between RT and 573°C is the result of the combination of the HQ and LQ behavior, depending on the inversion temperature.

The comparison for the cell parameters to the work of Zandona et al. [21] was chosen by the comparable, well-suited range of SiO_2 and Al_2O_3 for the investigated LAS system. The reader is also referred to the works of Xu et al. [38] and Zandona et al. [39] showing good agreement of the properties with the aforementioned reference.

3.4 | Modeling of Stresses

By the resemblance of the characteristic of the relative average change in unit cell lengths compared to the literature (see Figure 10A), a similar behavior of the thermal expansion of the investigated crystalline phases from the multicomponent glasses as for the ternary LAS system can be concluded.

Figure 11 presents the recalculated mean linear CTE values from crystallographic data from Zandona et al. [21] for the ternary LAS system in the temperature range of 25°C–560°C. Values for Al_2O_3 contents below 7.5 mol% were chosen to take the regime of compositions with no stabilization of the HQz-ss down to RT into account.

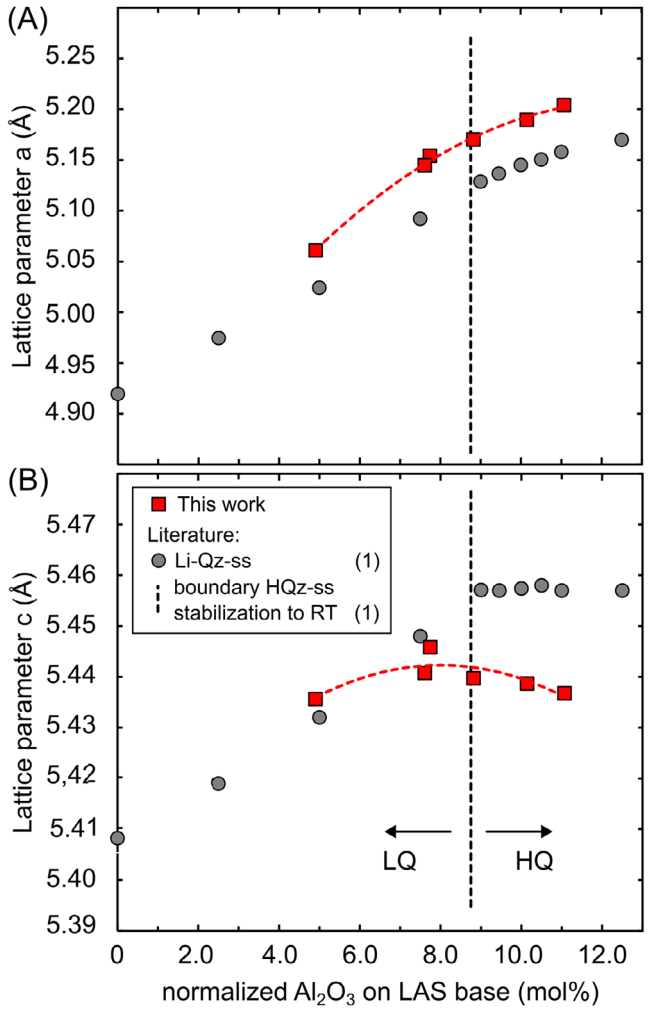

FIGURE 8 | Lattice parameters obtained for the formed Qz-ss of glasses G10–G15, depending on the normalized Al_2O_3 content in comparison to Qz-ss for the pure LAS system [21]. Polynomial fitting lines for guidance of the eye. Error bars are smaller than the depicted symbols. (A) Lattice parameter *a*. (B) Lattice parameter *c*.

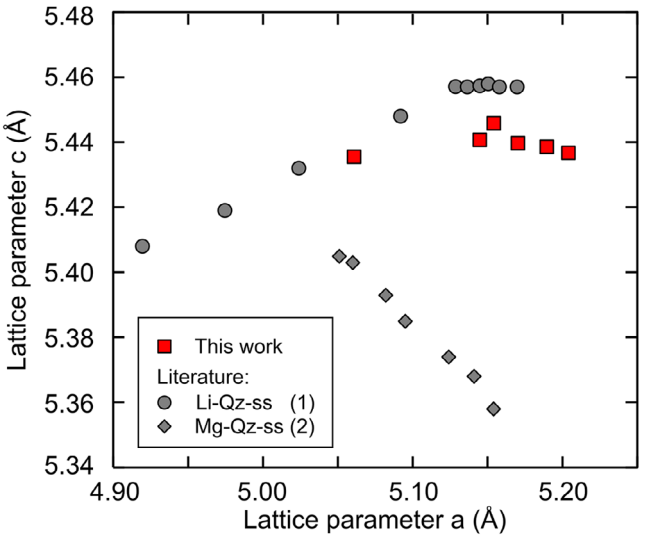

FIGURE 9 | Correlation between lattice parameters *a* and *c* of the Qz-ss crystallized in glasses G10–G15 compared to Qz-ss for the pure LAS (1) [21] and MAS system (2) [35]. Error bars are smaller than the depicted symbols.

In general, it can be assumed that for Al_2O_3 contents larger than 6.1 mol% CTE values for the crystalline phase below that for container SLS glass (~9.0•10^{-6} 1/K) [26] can be obtained. This would translate to an approximated Al_2O_3 content of larger 4.7 mol% and SiO_2 content of lower than 68 mol% in the glass with other oxide content levels as for glass G15 and lithium present in the exchange for sodium. However, the consumption of Li_2O, Al_2O_3, and SiO_2 during crystallization from the residual glass will generate a shift in composition of the residual glass phase. Based on glass composition G15, the following calculations show the combination of this influence with the anticipated effect of crystallization, depending on the Al_2O_3 content of the glass in the LQz-ss range. The Li_2O content in the layer before crystallization is an estimation by the salt treatment of an 88% exchanged fraction of Na^+ to Li^+. For the calculation chosen, molar compositions therefore are for the parent glass $(72.7\text{-}x)SiO_2$—xAl_2O_3—10CaO—3.5MgO—$13.8Na_2O$, respectively $(72.7\text{-}x)SiO_2$—xAl_2O_3—10CaO—3.5MgO—$1.7Na_2O$—$12.1Li_2O$ after the ion-exchange. Table 8 summarizes the variations used in the calculation. The stoichiometry of the Qz-ss is anticipated from the available SiO_2 and Al_2O_3 contents of the parent glass. The CTE values are predicted by the interpolation of the literature values from Figure 11. The densities of the crystalline phase are an interpolation of the x-ray densities obtained for the LQz-ss regime in Figure 10B.

Figure 12 shows an example of the calculated evolution of properties by the change in crystallized volume in the crystallized layer for a glass composition with $x = 4.7$.

The calculations with the variation of the Al_2O_3 content show that for glasses with Al_2O_3 contents lower than 5.5 mol% the dominating influence is the chemical shift in the residual glass of the crystallizing layer. The potentially formed compressive stress by initial Li^+ exchange ("glazing-effect") by the lower CTE of the exchange layer [5] is then reduced by further crystallization and changes of composition, especially the consumption of SiO_2, in the residual glass. This leads to an overall increase in the CTE of the crystallized layer with undesired lowering of potential compressive stress by the increased crystalline content. Figure 13 shows the calculated overall formed stresses in the crystallized layer during cooling from treatment temperature to RT, depending on *x*, the Al_2O_3 content in the glass.

In the context of obtaining a surface layer with a CTE lower than that of the parent glass over the full range of crystallization, an Al_2O_3 content of about 5.5 mol% or larger in the glass seems desirable. This translates to an Al_2O_3 content of 7.0 mol% referred to the normalized LAS system.

The calculated compressive stresses are in the range of those of thermal strengthening [40]. On the other hand, predicted compressive stresses are lower than for the classical chemical strengthening by IOX [2, 6]. The assumed compressive stress

TABLE 8 | Values used for the estimation of properties of the formed crystallized layer and prediction of resulting stresses.

Al_2O_3 content in glass (*x*) (mol%)	Normalized Al_2O_3 to LAS system (mol%)	Anticipated stoichiometry of crystalline phase			CTE crystalline phase (10^{-6} 1/K)	Density crystalline phase (g/cm³)
		SiO_2	Al_2O_3	Li_2O		
4.7	6.1	14.5	1	1	8.97	2.53
5.1	6.5	13.4	1	1	7.48	2.52
5.5	7.0	12.2	1	1	5.54	2.50
5.9	7.5	11.3	1	1	3.53	2.47

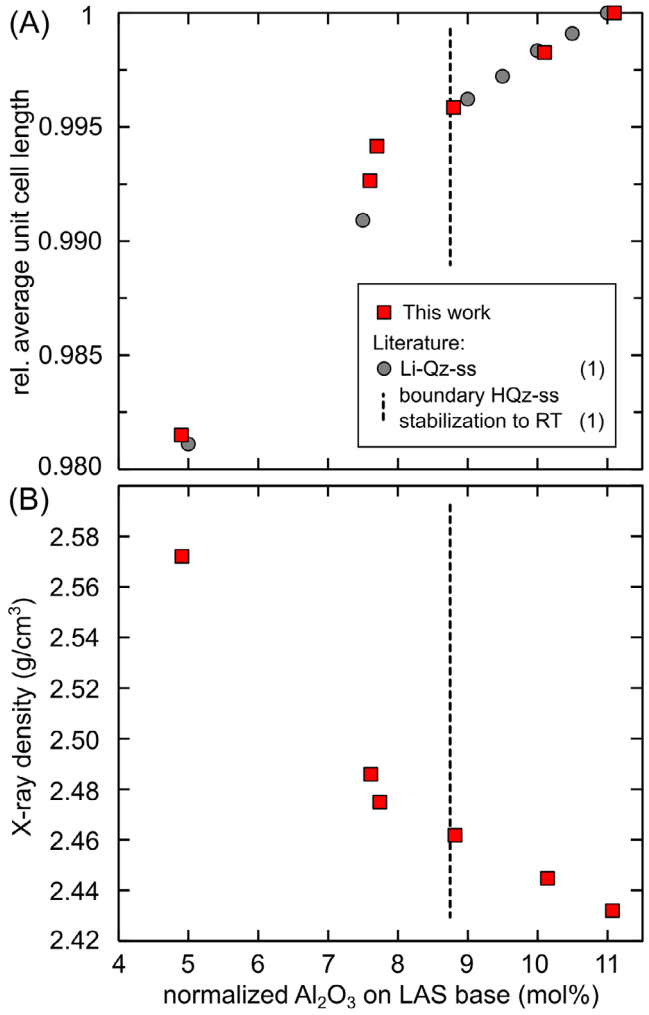

FIGURE 10 | Change of properties of the crystalline phase at room temperature with variation of the Al_2O_3 content in the glass, normalized to the LAS system. Comparison to data from literature (1) [21]. (A) Change of the relative average cell length normalized to one at an Al_2O_3 content of 11% of the LAS system. (B) Density of crystalline phases obtained from XRD measurements.

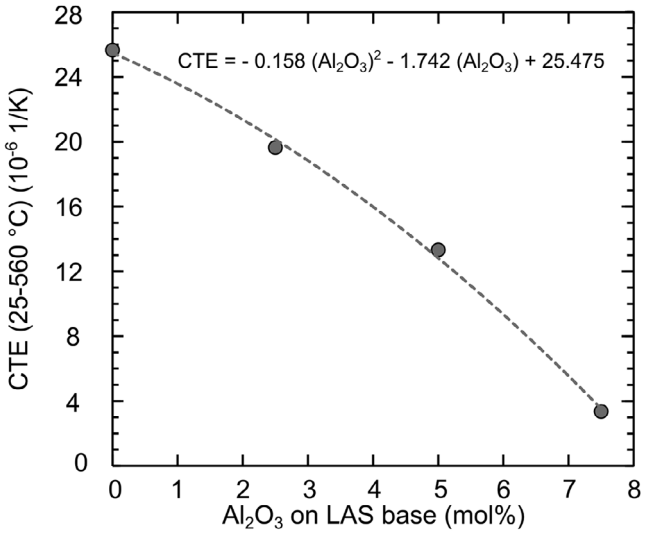

FIGURE 11 | Dependency of CTE (25°C–560°C) on the Al_2O_3 content of the Qz-ss of the pure LAS system, for the compositional range without stabilization of the HQz-ss down to RT. Recalculated from data of Zandona et al. [21].

resulting solely from the ion-exchange of sodium by lithium will be at about 75 MPa and is comparable to Company Vetropack's approach for thermal strengthening of container glass (~10–50 MPa) (by brand name Echovai), which has been proven to sufficiently improve properties of container glass [41].

The model shows that glass G15 should be seen as the most prospective composition of the investigated glasses, having an additional margin for strengthening. To match the model values to the actual obtained crystallization of this glass, the crystallization depth and fraction of the crystallization were further evaluated.

3.5 | Crystalline Surface Layer Characteristics of the Most Prospective Composition

The crystallization depth of the bulk sample of glass G15 was examined by optical microscopy. The cross-sectional fracture surface after described ion-exchange treatment and temperature program T6 shows a crystallization depth of about 35 µm on average (Figure 14).

The morphology of the crystal growth is of a spherulitic pattern starting at individual points of nucleation from the surface. This

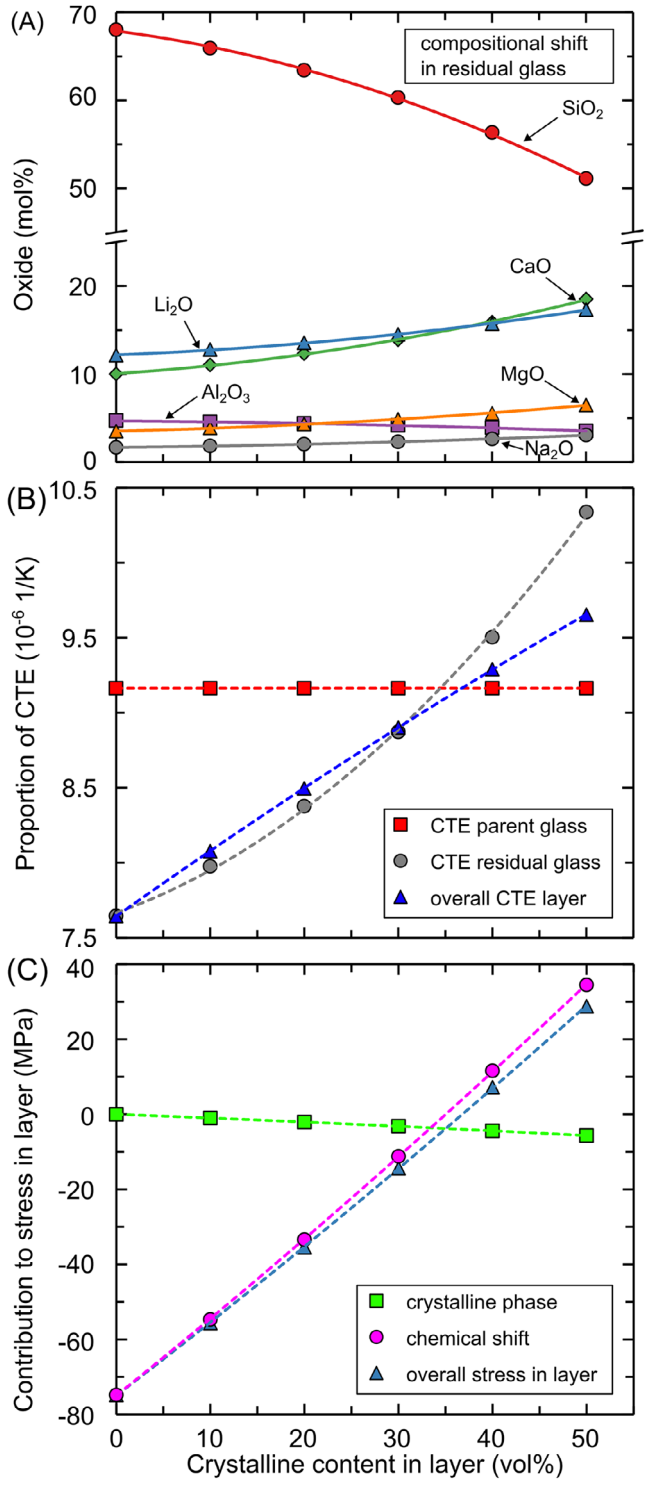

FIGURE 12 | Modeling of properties for an exemplary value $x = 4.7$ depending on the crystalline content in the formed layer. (A) Shift of the composition of the residual glass phase with increasing crystalline content. (B) Evolution of the different proportions of the CTE with variation of crystalline content used for calculation of the stresses (CTE of the parent glass, CTE of the residual glass, overall CTE including the crystalline phase). (C) Calculated stress in the crystallized layer for different crystalline contents as a result of the mismatch of CTE to the parent glass.

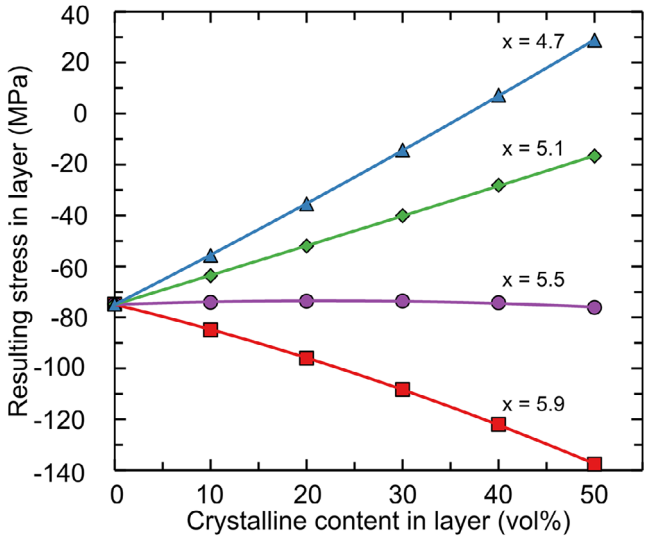

FIGURE 13 | Calculated resulting stresses in the crystallized layer depending on the crystalline content and the amount of Al_2O_3 *(x)* in the glass.

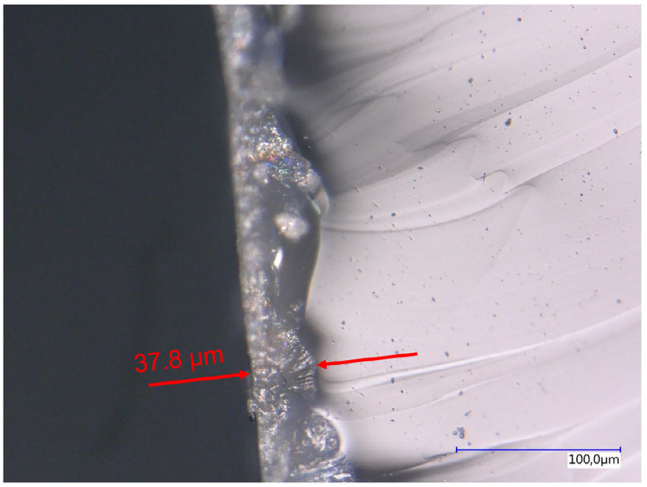

FIGURE 14 | Crystallization depth assessed by optical microscopy for the cross-section fracture plane of the bulk sample of glass G15 treated with salt mix and heat treatment T6.

is in agreement with the crystallization morphology described for surface crystallization of quartz by Lutjes et al. [42].

After milling the sample with Y_2O_3 (COD #152330) as an internal standard, a total of 1.1 wt% of Qz-ss crystalline phase with an estimated standard deviation of 0.19 wt% by quantitative XRD phase analyses was detected. Referred to the volume of the crystallized layer, and volume of the sample obtained by their thickness, the volume part of the crystalline phase in the crystallized layer was calculated to be 29.5 ± 5.1 vol%, assuming a density of 2.47 g/cm^3 for the crystalline phase. The obtained crystallization depth is comparable to the case depth for the classical IOX of sodium by potassium in molten salt baths for several hours [10, 43]. Based on the determined volume fraction of crystallization, the model predicts an induced compressive stress in the surface layer of approximately 124 MPa (SiO_2:Al_2O_3 ratio 10.9:1 with estimated CTE of crystalline phase of 2.53 10^{-6} 1/K).

The composition still has an increased Al_2O_3 content compared to standard soda-lime-silicate container glass. However, Fluegel model [44] calculated isokom temperatures at a viscosity of $\log(\eta/(\text{Pas})) = 1.5$ show a temperature increase of less than 50 K. While this increased melting temperature is unfavorable from a processing standpoint, the increased Al_2O_3 content should also be discussed in relation to other factors, as it offers further benefits beyond being strengthened through the surface crystallization. For example, it is also possible to reduce the CO_2 emissions of the batch by using a higher share of complex carbonate-free raw materials (e.g., feldspars, …). In addition, a positive effect on the hydrolytic resistance of the glass is expected.

4 | Conclusions

The study highlights the potential of strengthening glass through surface crystallization by establishing a compressive stress in the (partially) crystallized layer induced by the formed Qz-ss. Compared to former approaches for lithium-aluminosilicate-based compositions that stabilize the HQz-ss to room temperature and maximize the performance through relatively high Al_2O_3, our focus was on identifying compositions that are derived from soda–lime–silicate glass, can be strengthened through surface crystallization of Qz-ss, are cost-effective, and have the lowest possible alumina content.

For the investigated compositional range, we find that Al_2O_3 contents below the threshold to stabilization HQz-ss to RT (molar SiO_2:Al_2O_3-ratio < 12.2:1) might, in principle, feasible to obtain a crystalline phase with a sufficiently lower CTE than the parent glass. On the other hand, the chosen model also depicts the large influence of the change in CTE of the residual glass caused by the initial lithium-exchange and the later consumption of components during crystallization. Considering the possible uncertainty of the model, glass G15 therefore represents the most promising composition of the studied glasses, as it still offers additional margin for strengthening.

The investigated crystallization of Qz-ss seems dominated, but not exclusive, by the participation of SiO_2, Al_2O_3, and Li_2O. Despite the rather complex glass compositions, the obtained crystalline phases exhibit unit cell parameters close to those of the pure LAS system and are dictated by the stoichiometry of SiO_2:Al_2O_3 available in the glass (in the presence of lithium). The influence of additional ZnO and MgO in the glasses and their ratio on the crystalline phase is rather low.

With a crystallization depth of 35 µm, a thin, comparable to classical IOX, compressive layer thickness can be formed. The calculated compressive stresses are in the range of those for thermal strengthening, but with no limits on wall thickness and material distribution. The calculated compressive stresses are lower than for the classical chemical strengthening but might be established for the obtained case depth at way lower times. Despite the fact that Al_2O_3 contents in the glass lower than 5.5 mol% the overall compressive stress decreases in the model by the chemical shift in the residual glass, for a certain amount of crystalline phase, the approach still might be interesting, as also an increase in scratch resistance by the harder crystalline phase is expected.

The presented method can contribute to the development of optimized glasses that can be strengthened through surface crystallization. The discussed approach can also be extended to other compositions that exhibit crystallization of low-CTE phases and should encourage greater consideration of this method as an alternative to strengthening through classical ion-exchange and thermal tempering.

Acknowledgments

The authors are thankful for the funding by the Österreichische Forschungsförderungsgesellschaft (FFG) and Stoelzle Oberglas GmbH. Further gratitude is extended to the University of Bayreuth for supporting the publication through its Open Access Publishing Fund and to the Bavarian Academic Forum (BayWISS) for the financial support and for providing the cooperative framework of the research. In addition, the authors like to thank Stefan Zelder and Philipp Rank at Keylab Glass of the University of Bayreuth for their support with the XRD analyses and the Chair for Metals and Alloys of the University of Bayreuth for providing access to the XRD device for the measurements. Further, the authors would like to extend their gratitude to Tobias Helling of the Technology Application Center Spiegelau of the Deggendorf Institute of Technology for his help with the DTA measurements. We thank Thomas Scheibel for commenting on an earlier version of the manuscript and two anonymous reviewers for their valuable comments and suggestions.

Open access funding enabled and organized by Projekt DEAL.

Funding

The work was funded by the Österreichische Forschungsförderungsgesellschaft under grant (FFG-Basis) FO999917860 and by Stoelzle Oberglas GmbH. Publishing was funded by the Open Access Publishing Fund of the University of Bayreuth. Further funding was received from the Bavarian Academic Forum (BayWISS) for consortial doctorates.

Conflicts of Interest

The authors declare no conflicts of interest.

References

1. R. E. Mould, "The Strength of Inorganic Glasses," in *Fracture of Metals, Polymers, and Glasses* (Springer, 1967): 119–149.

2. S. Berneschi, G. C. Righini, and S. Pelli, "Towards a Glass New World: The Role of Ion-Exchange in Modern Technology," *Applied Science* 11 (2021): 4610, https://doi.org/10.3390/app11104610.

3. R. Gardon, "Thermal Tempering of Glass," *Glass Science and Technology* 5: 145–216, https://doi.org/10.1016/B978-0-12-706705-6.50010-2.

4. S. Karlsson, "Spontaneous Fracture in Thermally Strengthened Glass—A Review and Outlook," *Ceramics—Silikaty* 61 (2017): 188–201, https://doi.org/10.13168/cs.2017.0016.

5. G. Macrelli, Chemical Strengthening of Glass by Ion-Exchange, paper presented at the ICG Annual Meeting, Istanbul, Turkey, October 24, 2017.

6. S. Karlsson, B. Jonson, and C. Stålhandske, "The Technology of Chemical Glass Strengthening—A Review," *Glass Technology: European Journal of Glass Science and Technology Part A* 51, no. 2 (2010): 43–54.

7. J. E. Lee, H.-T. Im, H. S. Kim, et al., "Effect of α-Al_2O_3 Particle Size in a Slurry on the Physical Properties of Chemically Strengthened Thin Glass Prepared by the Spray Method," *ACS Omega* 5 (2020): 26667–26672, https://doi.org/10.1021/acsomega.0c03518.

8. K. W. Min, J. H. Choi, Y. Jung, Y. M. Byun, W. B. Im, and H.-J. Kim, "Weibull Reliability and Mechanical Properties of Chemical Strength-

ening Lightweight Glass Containers Using Spray Coating," *Processes* 11 (2023): 15, https://doi.org/10.3390/pr11010015.

9. E. M. Aaldenberg, P. J. Lezzi, J. H. Seaman, T. A. Blanchet, and M. Tomozawa, "Ion-Exchanged Lithium Aluminosilicate Glass: Strength and Dynamic Fatigue," *Journal of the American Ceramic Society* 99 (2016): 2645–2654, https://doi.org/10.1111/jace.14294.

10. İ. Erdem, D. Guldiren, and S. Aydin, "Chemical Tempering of Soda Lime Silicate Glasses by Ion Exchange Process for the Improvement of Surface and Bulk Mechanical Strength," *Journal of Non-Crystalline Solids* 473 (2017): 170–178, https://doi.org/10.1016/j.jnoncrysol.2017.08.010.

11. C. Ragoen, S. Sen, T. Lambricht, and S. Godet, "Effect of Al_2O_3 Content on the Mechanical and Interdiffusional Properties of Ion-Exchanged Na-Aluminosilicate Glasses," *Journal of Non-Crystalline Solids* 458 (2017): 129–136, https://doi.org/10.1016/j.jnoncrysol.2016.12.019.

12. D. W. Rinehart, Surface Crystallized Glass and Method of Producing (PPG Industries Inc.) US 3,464,880 (United States Patent and Trademark Office, 1969).

13. J. S. Olcott and S. D. Stookey, "Glass Body Having a Semicrystalline Surface Layer and Method of Making it (Corning Glass Works) US 2,998,675," (United States Patent and Trademark Office, 1961).

14. G. J. Fine and M. E. Greene, Strong, Surface Crystallized Glass Articles (Corning Incorporated) US 5,084,328 (United States Patent and Trademark Office, 1992).

15. K. K. Mallick and D. Holland, "Strengthening of Container Glasses by Ion-Exchange Dip Coating," *Journal of Non-Crystalline Solids* 351 (2005): 2524–2536, https://doi.org/10.1016/j.jnoncrysol.2005.06.040.

16. S. Priller, G. H. Frischat, and L. D. Pye, "Strengthening of Glass Through Surface Crystallization of β-Spodumene SS," *Journal of Non-Crystalline Solids* 196 (1996): 144–149.

17. J. Yang, J. Xing, Q. Zheng, A. Qiao, and H. Tao, "Transparent Surface Crystallized Aluminosilicate Glasses With an Ultrahigh Crack Resistance," *Journal of Non-Crystalline Solids* 635 (2024): 122996, https://doi.org/10.1016/j.jnoncrysol.2024.122996.

18. D. C. N. Fabris, E. H. Miguel, R. Vargas, et al., "Microstructure, Residual Stresses, and Mechanical Performance of Surface Crystallized Translucent Glass-Ceramics," *Journal of the European Ceramic Society* 42 (2022): 4631–4642, https://doi.org/10.1016/j.jeurceramsoc.2022.04.024.

19. S. Karlsson, "Viscosity of Alumina Doped Soda Lime Silicate Glasses—Observation of Anomaly in the Linear Increase as Al_2O_3 Replaces SiO_2," *Journal of Non-Crystalline Solids* 573 (2021): 121149, https://doi.org/10.1016/j.jnoncrysol.2021.121149.

20. Z. Xiao, J. Cheng, and H. Wu, "Effect of Al_2O_3/SiO_2 Ratio on the Viscosity and Workability of High-Alumina Soda–Lime–Silicate Glasses," *Journal of the Chinese Ceramic Society* 40 (2012): 1000–1005.

21. A. Zandona, G. Helsch, A. M. Arias, A. P. Weber, and J. Deubener, "Spray-Dried Sol–Gel Glass-Ceramic Powders Based on the Tunable Thermal Expansion of Quartz and Keatite Solid Solutions," *Journal of the American Ceramic Society* 105 (2022): 207–216, https://doi.org/10.1111/jace.18057.

22. N. Doebelin and R. Kleeberg, "Profex: A Graphical User Interface for the Rietveld Refinement Program BGMN," *Journal of Applied Crystallography* 48 (2015): 1573–1580, https://doi.org/10.1107/S1600576715014685.

23. J. W. Hutchinson, *Stresses and Failure Modes in Thin Films and Multilayers* (Technical University of Denmark, Notes for DCAMM Course, 1996).

24. A. A. Appen, *Khimiya stekla (Chemistry of Glass)* (Khimiya Publishing House, 1974).

25. Schott AG, ZERODUR® Glass-Ceramic With Near-Zero Thermal Expansion, Schott AG, accessed July 15, 2025, https://www.schott.com/en-gb/products/zerodur-p1000269/downloads.

26. J. E. Shelby, *Introduction to Glass Science and Technology*, 2nd ed. (Royal Society of Chemistry, 2005).

27. A. Fluegel, "Global Model for Calculating Room-Temperature Glass Density From the Composition," *Journal of the American Ceramic Society* 90 (2007): 2622–2625, https://doi.org/10.1111/j.1551-2916.2007.01751.x.

28. B. P. Da Fonseca, G. Helsch, A. Zandonà, and J. Deubener, "Crystallographic Assessment and Thermal Expansion Fine-Tuning of Quartz Solid Solutions in the ZnO—MgO—Al_2O_3—SiO_2 System," *Journal of the American Ceramic Society* 108 (2024): e20314, https://doi.org/10.1111/jace.20314.

29. J. Petzold, "Metastabile Mischkristalle mit Quarzstruktur mit Oxidsystem Li_2O—MgO—ZnO—Al_2O_3—SiO_2," *Glastechnische Berichte* 40 (1967): 385–396.

30. S. Ray and G. M. Muchow, "High-Quartz Solid Solution Phases From Thermally Crystallized Glasses of Compositions (Li_2O, MgO).Al_2O_3,nSiO_2," *Journal of the American Ceramic Society* 51 (1968): 678–682, https://doi.org/10.1111/j.1151-2916.1968.tb15927.x.

31. H. Xu, P. J. Heaney, and A. Navrotsky, "Thermal Expansion and Structural Transformations of Stuffed Derivatives of Quartz Along the $LiAlSiO_4$—SiO_2 Join: A Variable-Temperature Powder Synchrotron XRD Study," *Physics and Chemistry of Minerals* 28 (2001): 302–312, https://doi.org/10.1007/s002690100165.

32. L. Cormier, L. Delbes, B. Baptiste, and V. Montouillout, "Vitrification, Crystallization Behavior and Structure of Zinc Aluminosilicate Glasses," *Journal of Non-Crystalline Solids* 555 (2021): 120609, https://doi.org/10.1016/j.jnoncrysol.2020.120609.

33. H. Xu, X. Lü, P. J. Heaney, and Y. Ren, "Structural Behavior of a Stuffed Derivative of α-Quartz, $Mg0.5AlSiO_4$, at High Temperature: An In Situ Synchrotron XRD Study," *Physics and Chemistry of Minerals* 46 (2019): 717–725, https://doi.org/10.1007/s00269-019-01033-1.

34. J. Kjeldsen, M. M. Smedskjaer, J. C. Mauro, R. E. Youngman, L. Huang, and Y. Yue, "Mixed Alkaline Earth Effect in Sodium Aluminosilicate Glasses," *Journal of Non-Crystalline Solids* 369 (2013): 61–68, https://doi.org/10.1016/j.jnoncrysol.2013.03.015.

35. A. Zandona, B. Rüdinger, and J. Deubener, "Mg-Bearing Quartz Solid Solutions as Structural Intermediates Between Low and High Quartz," *Journal of the American Ceramic Society* 104 (2021): 1146–1155, https://doi.org/10.1111/jace.17517.

36. A. Zandonà, B. Da Paiva Fonseca, G. Helsch, et al., "Structural Features and Thermal Expansion of Zinc Aluminosilicate Quartz Solid Solutions," *Journal of the European Ceramic Society* 44 (2024): 7769–7777, https://doi.org/10.1016/j.jeurceramsoc.2024.05.046.

37. A. Zandona, G. Helsch, R. Al-Mukadam, and J. Deubener, "The Effects of a Li_2O Excess on the Crystallization Sequence of Lithium Aluminosilicate Glass Powders," *Journal of Non-Crystalline Solids* 561 (2021): 120748, https://doi.org/10.1016/j.jnoncrysol.2021.120748.

38. H. Xu, P. J. Heaney, and G. H. Beall, "Phase Transitions Induced by Solid Solution in Stuffed Derivatives of Quartz: A Powder Synchrotron XRD Study of the $LiAlSiO_4$—SiO_2 Join," *American Mineralogist* 85 (2000): 971–979, https://doi.org/10.2138/am-2000-0711.

39. A. Zandona, G. Helsch, and J. Deubener, "Inversion of Quartz Solid Solutions at Cryogenic Temperatures," *Journal of the American Ceramic Society* 103 (2020): 6630–6638, https://doi.org/10.1111/jace.17393.

40. L. Efferz, K. Thiele, M. Schuster, C. Schuler, G. Siebert, and J. Schneider, "Relation Between Edge Stress, Bending Strength, Surface Stress and Fracture Pattern of Thermally Toughened Glass," *Glass Structures & Engineering* 9 (2024): 307–320, https://doi.org/10.1007/s40940-024-00269-w.

41. D. Egger, *Das Echovai Verfahren (The Echovai process), Fachausschusssitzung FA IV* (Deutsche Glastechnische Gesellschaft, 2023).

42. N. R. Lutjes, S. Zhou, J. Antoja-Lleonart, B. Noheda, and V. Ocelík, "Spherulitic and Rotational Crystal Growth of Quartz Thin Films,"

Scientific Reports 11 (2021): 14888, https://doi.org/10.1038/s41598-021-94147-y.

43. S. Karlsson and B. Jonson, "Surface Analysis of Float Glass Using Surface Ablation Cell (SAC). Part 2. Determination of the Diffusion Characteristics of K^+-Na^+ Ion Exchange," *Glass Technology: European Journal of Glass Science and Technology Part A* 51, no. 2 (2010): 55–62.

44. A. Fluegel, "Glass Viscosity Calculation Based on a Global Statistical Modelling Approach," *Glass Technology: European Journal of Glass Science and Technology Part A* 48 (2007): 13–30.

Supporting Information

Additional supporting information can be found online in the Supporting Information section.

Supporting Information file 1: ijag70023-sup-0001-SuppMat.xlsm